CANADIAN JOURNAL OF EXPLORATION GEOPHYSICS
VOL. 33, NOS 1 & 2 (DECEMBER 1997), P. 1-7

AN EXAMPLE OF THE COMPUTATION OF EDGE DIFFRACTED WAVES

J.B. GALLOP AND F. HRON

ABSTRACT

We present the application of the theory of edge diffracted waves to the Amoco model, for the P-SV case. We show how to calculate some of the terms in the edge wave formulation, including wave polarization, and the continuation of both the geometrical eikonal and geometrical amplitude into the shadow zone. Seismograms from zero order Asymptotic Ray Theory were computed both with and without edge waves, to show how necessary the latter are to complete the solution. We focus on the step by step construction of a smooth solution for two of the arrivals using a combination of edge waves. This provides insight into the conditions present in the zero order solution which indicate the presence of diffracted waves. It also demonstrates a limitation of the theory of edge waves in a complex model; specifically, when shadow boundaries approach interfaces tangentially, boundary conditions are not satisfied by the edge waves. Finally, we give an example of a situation involving interface complications, where a subset of primary diffracted waves cannot be described using the edge wave formulation.

INTRODUCTION

The lack of a useful description for diffracted waves in Asymptotic Ray Theory (ART) has been a drawback of the method for many years. Keller (1962) originally proposed the geometrical theory of diffraction which corrected some of the shortcoming. However, these diffracted waves depend on a diffraction coefficient (essentially a directivity pattern) which is singular at the shadow boundary, the surface dividing the illuminated and the shadow zones. They also do not rectify the discontinuity in the geometrical wave (the zero order ART solution) located at the shadow boundary. Boundary layer techniques (see for example Zauderer, 1990) can be applied in the narrow region surrounding the shadow boundary. Klem-Musatov (1984) and Bakker (1990) have successfully derived the shadow boundary layer solution for seismic diffracted waves (edge waves) in a convenient, general form to be used in conjunction with ART. Klaeschen et al. (1994) have developed a scheme to incorporate these diffracted waves into existing automatic ray tracing programs. The application of the theory of edge waves to a particular model can be complex, so we present an example here to examine some of the details. In this way we can appreciate the usefulness of edge waves in models that generate significant diffractions, and also look at some of the limitations of the theory, keeping in mind more general geologic situations. A summary of the theory of diffracted edge waves, including elaboration of some technical points, is given in Appendix A. In places it will be necessary to look at the formulation for diffracted waves, and here we shall refer to equations of Appendix A.

NUMERICAL EXAMPLE

The example we present employs the Amoco model used earlier by Hron and Chan (1994), who studied SH diffracted waves. It is a simplified version of a tar sands deposit in northern Alberta, which was used by Amoco researchers to determine the experimental and theoretical role of diffracted waves in field records (Hron and Covey, 1988). Here we investigate the P-SV case rather than the SH case. The model itself (Figure 1) is two dimensional and is composed of a box shaped low velocity zone embedded in a constant velocity layer between two half spaces. The vertical component receivers and the impulsive source are buried to avoid free surface effects. The ratio of P-wave to S-wave speeds is $\sqrt{3}$. The source wavelet is described by:

$$f(t) = A \sin(2\pi t)e^{-(\frac{\pi}{2}t)^2} \qquad (1)$$

where A is constant. Multiples and head waves were not calculated in the seismograms. Figure 2 contains the zero order ART results for this model. There are 12 geometrical body waves calculated here (each with a different type of raypath), and the dominant six are labelled. Figure 3 contains the ray diagrams corresponding to these arrivals. Many discontinuities are present in Figure 2, and it is clear that standard ART provides a very unsatisfactory solution. The wavefield with diffractions included (Figure 4) has all discontinuities smoothed using 30 unique diffracted wave contributions (each one is defined by the geometrical body wave discontinuity it smooths). The advantage of the Amoco model is that it presents several different cases of diffraction and we can use these to study the application of diffracted waves. We shall look at two arrivals in a detailed manner.

Department of Physics, University of Alberta, Edmonton, Alberta, Canada T6G 2J1

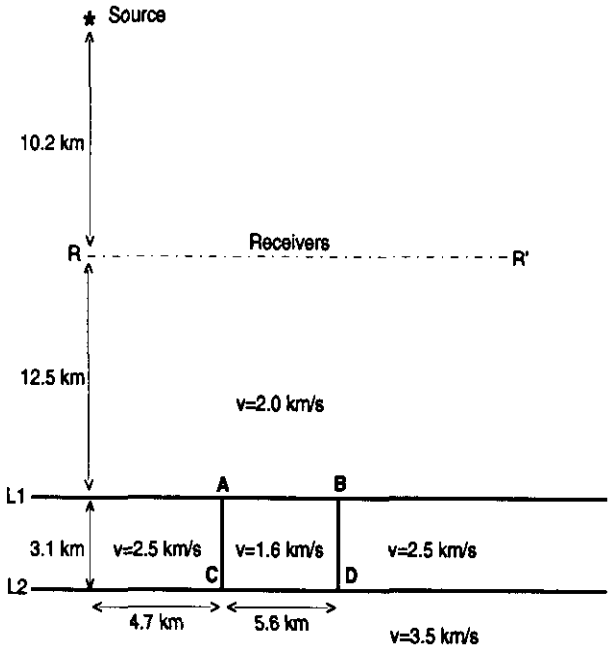

Fig. 1. The so called Amoco model used for computation of synthetic seismograms. The densities are equal to unity everywhere. The speeds indicated are for P-waves. The line RR' represents 60 equally spaced vertical displacement geophones.

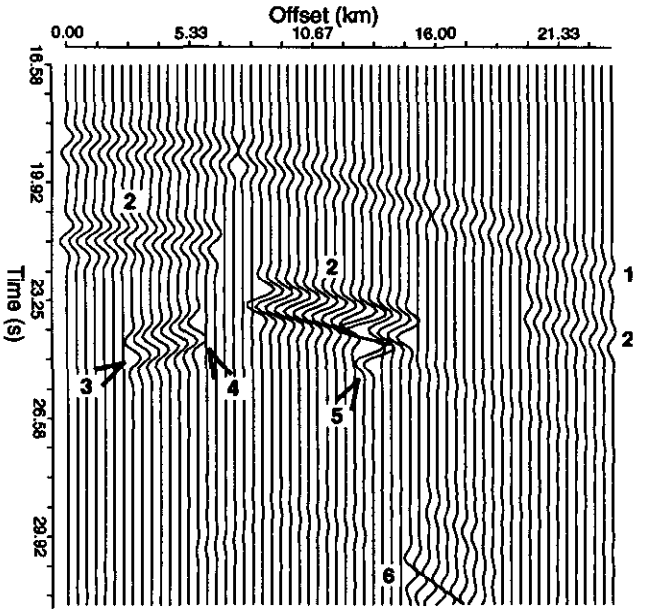

Fig. 2. The zero order ART response to the Amoco model. No multiples or diffractions are included. The six largest contributions are labelled here and described in the text. Their raypaths (using corresponding labels) can be found in Figure 3.

The first is a P-wave reflection from interface L2, labelled (2) in Figure 2. The geometrical rays (Figure 3) are completely truncated by the vertical interfaces AC and BD. The corner which terminates the reflections (A or B) gives rise to diffracted waves which smooth the transition from the presence to the absence of a reflection. The geometrical eikonal and amplitude are discontinuous across the shadow boundary, which divides the illuminated and shadow zones. The shadow boundary is represented by the last ray in the geometrical set of rays which approach the diffracting corner from a particular direction. In Figure 5 (bottom) we see the effect of adding the diffracted waves (labelled 2a) generated when the shadow boundary ray is the last geometrical ray whose path lies to the left of the vertical interface. Figure 5 (top) is a ray diagram illustrating this. The geometrical reflection is still incomplete, and more diffracted waves are needed. The last geometrical ray lying to the right of the vertical boundary (top of Figure 6) is a shadow boundary ray, and when we include the diffractions caused by it (labelled 2b) the zero order approximation reflection becomes nearly complete (bottom of Figure 6). There still exists a small discontinuity in the wavefield, located around 23 seconds at an offset of 4.7 km. It is here that the diffracted waves (2b) are themselves truncated by the vertical interface AC. We can introduce secondary diffracted waves at point A corresponding to the rays in Figure 7 (top) to smooth this. The shadow boundary ray in this case is a primary diffracted ray that travels vertically down from the point of diffraction (A), reflects at the interface L2 and travels upwards striking point A again causing secondary diffracted waves. The result is

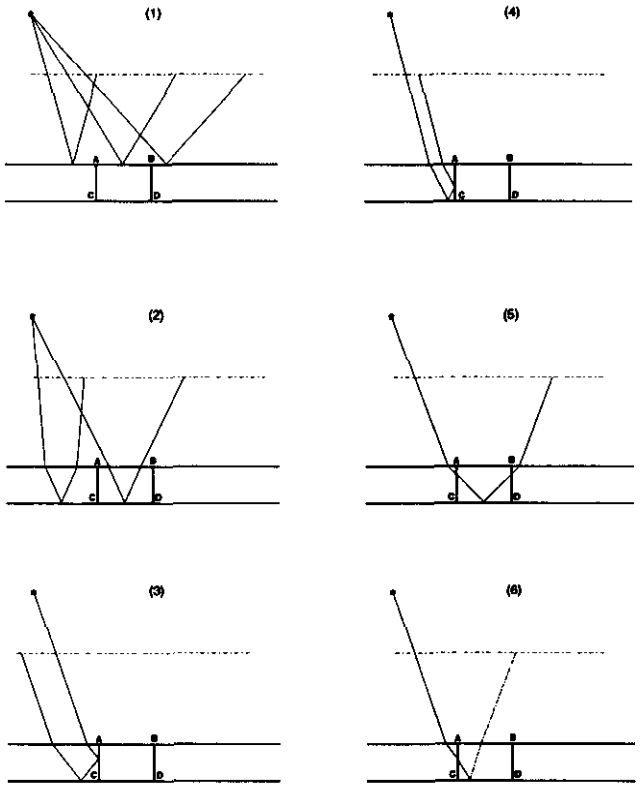

Fig. 3. Ray diagrams containing sample rays for the six dominant arrivals of zero order ART for the time frame shown in Figure 2. Diagrams are not to scale. All arrivals are P-waves except (6), where the dashed ray segment indicates conversion to an S-wave. The numbers shown correspond to the labels in Figure 2.

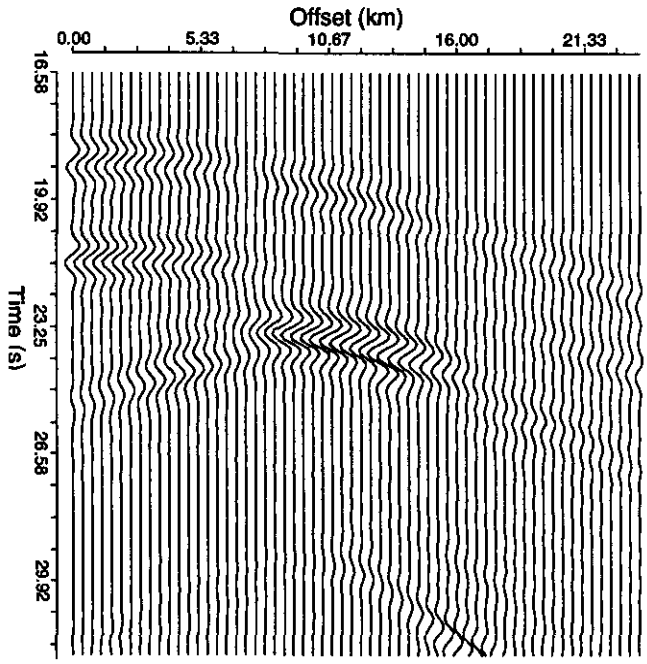

Fig. 4. The zero order ART solution to the Amoco model with diffracted waves included. Careful application has removed all discontinuities from the zero order ART solution.

shown in Figure 7 (bottom) and labelled (2c). Although these particular secondary diffracted waves seem to complete the wavefield adequately, we expect some additional error has been introduced. This is because the shadow boundary ray travels along the interface AC, and boundary conditions are not satisfied here without the presence of another wave travelling along the left side of AC. In our numerical example this is a relatively small defect, since the amplitude along the boundary ray in Figure 7 is low (it is near the edge of the shadow boundary layer). However, this represents one of the limits from the theory of edge waves; specifically, when an interface runs nearly parallel to a shadow boundary ray, boundary conditions are not satisfied and equation (A-3) is not correct to $O(1/\sqrt{\omega})$. (Equation (A-3) gives the formula for geometric and diffracted waves in the boundary layer).

The second case we shall consider is the P-wave reflection from the top interface L1 (labelled (1) in Figure 2). The shadow boundaries are defined by the rays reflecting from interface L1 at the points A and B. Unlike reflection (2), across the shadow boundaries the eikonal for reflection (1) is continuous and the geometrical wave doesn't vanish (it changes amplitude according to its reflection coefficient). The solution offered by equation (A-3) decays to zero in the shadow zone (see Figure 10), where no geometrical wave exists. In Figure 2 we see that a geometrical wave is present on both sides of the shadow boundary, the latter being visible in the seismograms where there is a reversal of polarity in the reflection. Hence to use equation (A-3) we need to break up the reflection into reflected ray groups lying to the left and right of each corner. Each of the two groups is defined by the continuity of its reflection coefficient. Kinematically each

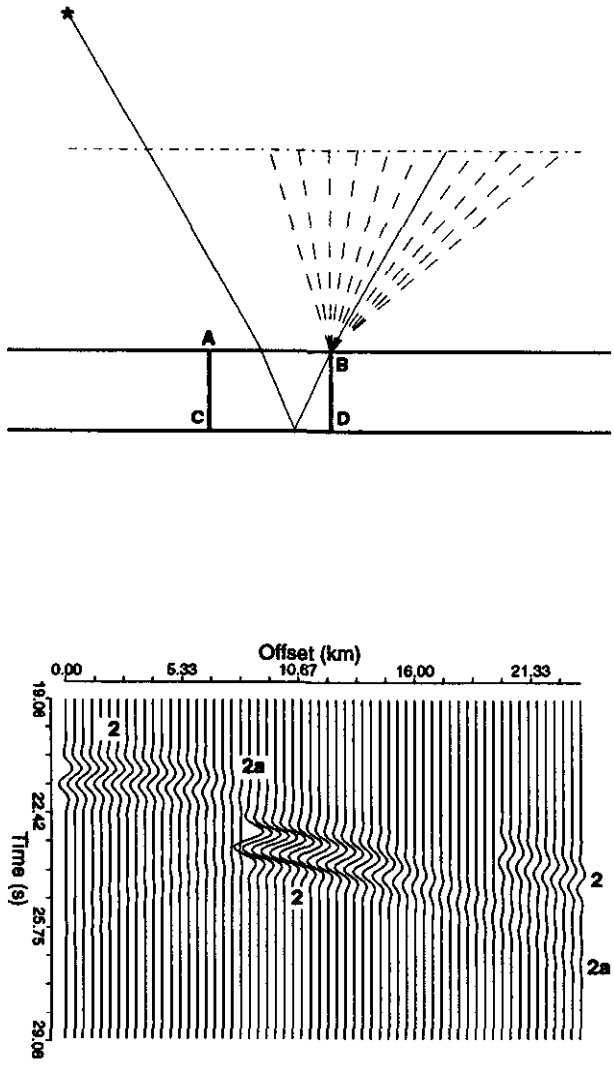

Fig. 5. (top) Ray diagram (not to scale) showing the diffracted rays (dashed) from point B that smooth arrival (2), the P-wave reflection from the bottom interface (L2). The boundary ray is shown as the solid line. Note that diffractions of the same type occur at corner A. (bottom) Seismograms of the geometrical arrival (2) with diffracted waves from corners A and B, labelled (2a).

group is identical at the shadow boundary, leading to a continuous eikonal. Focussing on corner A (which produces the leftmost discontinuity in reflection (1) in Figure 2), we can use equation (A-3) by first making $\tilde{U}_o$ the geometrical amplitude associated with the rays reflecting from interface L1 to the left of point A. The diffracted amplitude decays in the shadow zone to the right of the shadow boundary ray (Figure 8, top). Similarly, for the other diffracted wave we make $\tilde{U}_o$ the geometrical amplitude associated with the rays reflecting to the right of point A (see Figure 8, bottom). We can now appeal to the principal of superposition and combine the two as shown in Figure 4, where there is a smooth transition from one reflection coefficient to another across the shadow boundary. In our model the change in polarity emphasizes this transition.

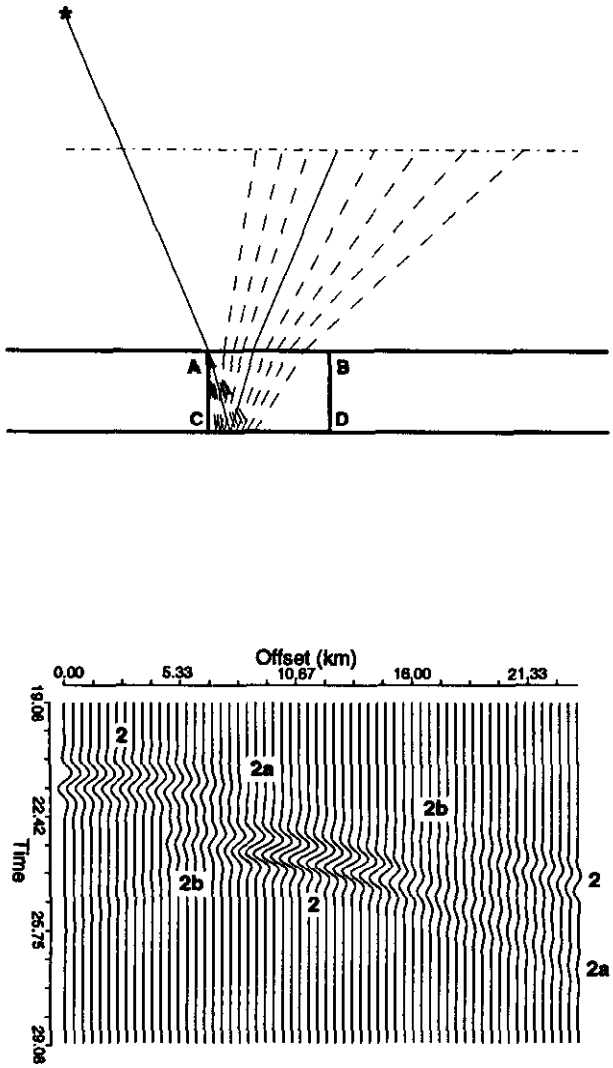

Fig. 6. (top) A ray diagram for the diffracted waves (dashed) originating at point A that smooth arrival (2). The boundary ray is shown as the solid line. Similar diffractions originate at corner B. (bottom) Seismograms of the geometrical arrival including the diffracted wave (2a) and the above type of diffracted wave, labelled (2b).

The previous two examples demonstrate that the presence of diffracted waves can be identified by sharp changes in geometrical wave amplitude or travel time. This fact was recognized by Klaeschen et al. (1994), and used in their automated 2-D ray tracing scheme which augmented standard ray theory with diffracted waves.

Interface Complications

The model we have used contains no significant interface complications as defined in the previous sections. However, we can adjust the model to consider how these complications might arise. Consider the shadow boundary shown in Figure 6, which is due to the reflected P-wave from interface L2. If we move the vertical interface BD closer to AC the result would look like the situation in Figure 9. The shaded area represents the boundary layer, where the diffracted waves are of significant amplitude. The model without adjustment had no diffracted rays in the boundary layer intersecting BD. One can see that for the rays intersecting the vertical interface BD the amplitude cannot be continued from the shadow boundary ray (the solid ray in Figure 9) as they have, for example, very different reflection transmission coefficients if boundary conditions are to be satisfied on BD. Also the description of diffracted waves given by equation (A-3) is no longer valid for the primary diffracted rays passing through BD, once they have transmitted through the top (L1) interface. The secondary diffracted waves from point B smooth the discontinuity in the primary diffracted waves that transmit through L1 to the left of B; hence the primary diffracted waves that transmit to the right of B no longer smooth any discontinuity, and cannot be represented by the form given in equation (A-3).

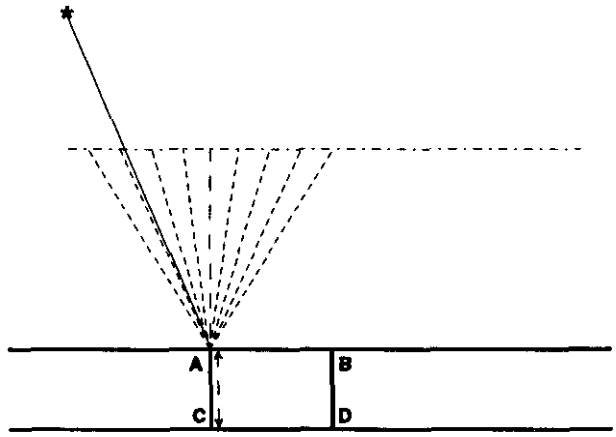

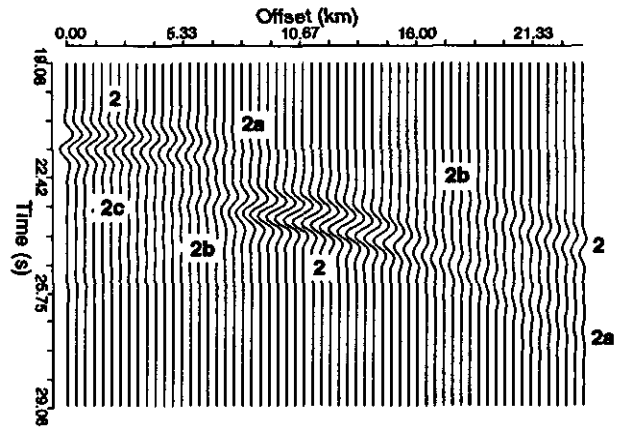

Fig. 7. (top) Ray diagram of doubly diffracted waves. The geometrical ray (solid) is diffracted at point A and travels vertically downwards (long dash). It then reflects at the bottom interface, travels upwards to point A creating secondary diffracted rays (short dash). (bottom) Seismograms including the geometrical wave (2), diffracted waves (2a) and (2b) and the above doubly diffracted wave, labelled (2c).

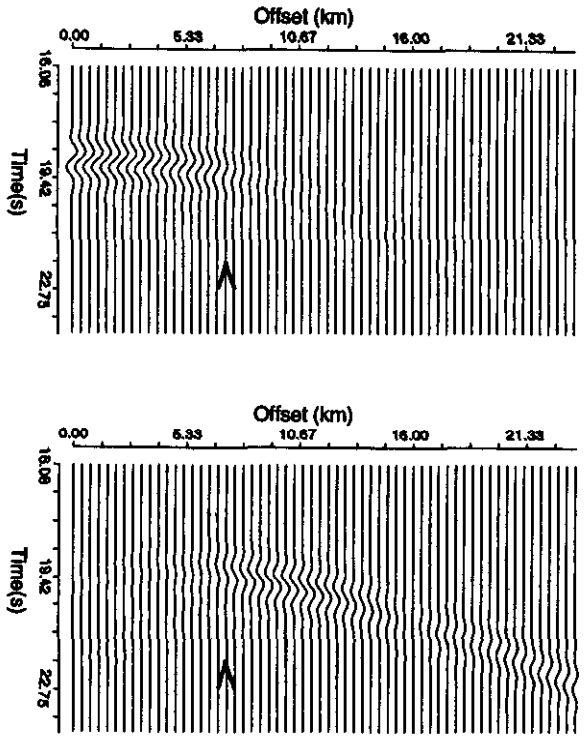

Fig. 8. (top) Seismograms of the geometrical arrival (1), the P-wave reflection from the top interface (L1), for the group of rays reflecting to the left of point A. Included are diffracted waves from A which smooth this arrival and decay to the right (the shadow zone for this group). (bottom) Seismograms of the geometrical arrival (1), for the rays reflecting to the right of point A including the diffracted waves from point A which smooth this arrival and decay to the left (into the shadow zone for this group). (Diffracted waves from point B have been used to make the bottom seismograms fully continuous.) The arrows indicate the position of the shadow boundary being examined.

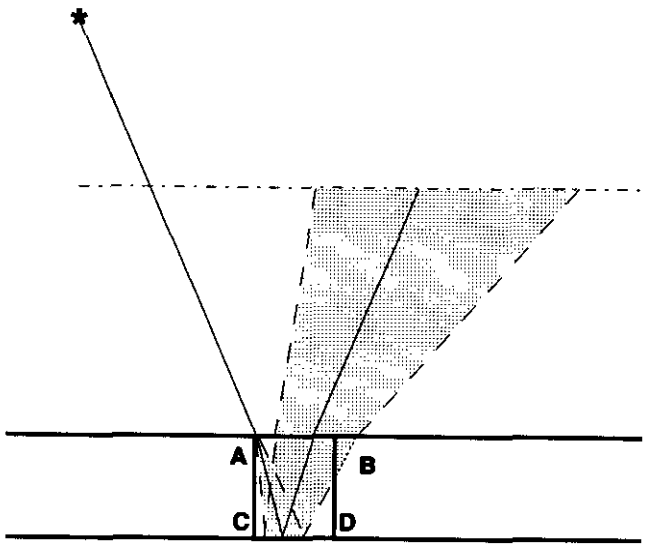

Fig. 9. A ray diagram illustrating where boundary complications might arise. Interface BD has been moved to the left to intersect the boundary layer (shaded) caused by the diffraction of waves at point A. The solid ray represents the shadow boundary ray.

CONCLUSIONS

We have shown using the Amoco model, one which generates significant diffractions, that the zero order ART solution for P-SV waves can be greatly improved through the use of the theory of edge waves. The diffracted waves smooth the many discontinuities present in the geometrical solution, leading to a continuous wavefield (which is to be expected based on the properties of the wave equation). The final solution must be composed of many diffracted waves from the same

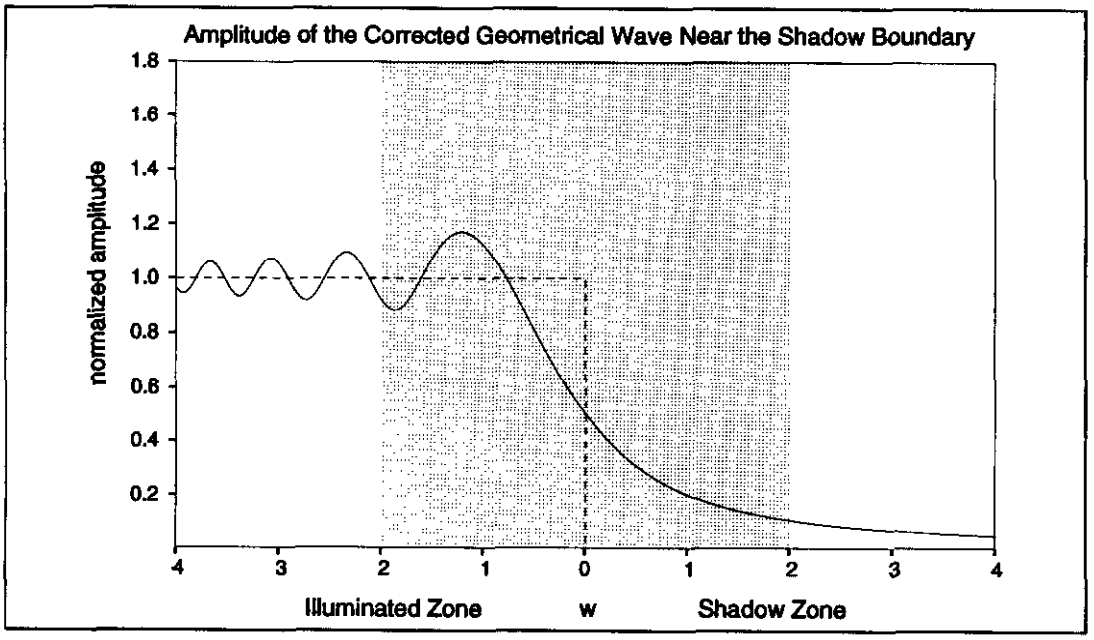

Fig. 10. Modulus of the normalized geometrical amplitude with diffracted waves included. The dashed line represents the geometrical amplitude without diffracted waves. The shaded area represents the shadow boundary layer, usually taken as $w < 2$.

point, each smoothing a particular geometrical ray group, the latter being defined by the continuity of geometrical amplitude. Through looking at individual diffracted ray groups we saw an instance of edge waves providing an incorrect solution, where a shadow boundary ran nearly parallel to an interface (and boundary conditions were not satisfied). Although rare, such situations are bound to arise in most complicated models, and should be identified to locate possible errors in seismograms. In the case of the Amoco model the error was negligible, since the affected edge waves were near the edge of the boundary layer where amplitudes are relatively low. Also we presented an instance where the original formulation of edge diffracted waves given by Klem-Musatov (1984), no longer applies. This occurs for a subset of primary diffracted waves when they encounter a new diffraction point (source of diffracted waves) during the course of prapagation.

Acknowledgment

Thanks to Roger Chan for the use of some Fortran subroutines from his doctoral thesis. This work was supported by a University of Alberta Ph.D. Scholarship and by NSERC operating grant 9157.

References

Bakker, P.M., 1990, Theory of edge diffraction in terms of dynamic ray tracing: Geophys. J. Int., **102**, 177-189.

Červený, V., and Hron, F., 1980, The ray series method and dynamic ray tracing system for three-dimensional inhomogeneous media: Bull. Seism. Soc. Am., **70**, 44-77.

_____ and Ravindra, R., 1971, Theory of seismic head waves: University of Toronto Press.

Hron, F. and Chan, G.H., 1995, Tutorial on the numerical modelling of edge diffracted waves by the ray method: Studia geoph. et geod., **39**, 103 - 137.

_____ and Covey, J.D., Theory of seismic waves diffracted by the linear edges of seismic interfaces: Technical Report F88-E-13, Amoco Research Center, 1988.

_____ and Kanasewich, E.R., 1971, Synthetic seismograms for deep sounding studies using asymptotic ray theory: Bull. Seism. Soc. Am., **61**, 1169-1200.

Keller, J.B., 1962, Geometrical theory of diffraction: J. Opt. Soc. Am., **52**, no. 2, 116-130.

Klaeschen, D., Rabbel, W. and Fluch, E., 1994, An automated ray method for diffraction modelling in complex media: Geophys. J. Int., **116**, 23-28.

Klem-Musatov, K.D. and Aizenberg, A.M., 1984, The ray method and the theory of edge waves: Geophys. J. R. astr. Soc., **79**, 35-50.

_____, 1994, Theory of seismic diffractions: Society of Exploration Geophysicists.

Zauderer, E., 1989, Partial differential equations of applied mathematics: John Wiley and Sons.

Appendix – Review of Theory

For complete review of ART see, for example, Hron and Kanasewich (1971). Let us represent the zero order ART contribution to a given model as $\mathbf{u} = U_o e^{i\omega\tau}\mathbf{e}$. Here we are working in the frequency domain where the angular frequency is ω and τ is the eikonal which satisfies

$$\nabla\tau\cdot\nabla\tau = \frac{1}{\upsilon^2} \qquad \text{(A-1)}$$

where υ is the speed of the isotropic, perfectly elastic media. U_o is the geometrical wave amplitude and obeys the transport equation

$$2\nabla\tau\cdot\nabla U_o + U_o\nabla^2\tau = 0. \qquad \text{(A-2)}$$

Unit vector **e** denotes the polarization of the wave displacement; this is parallel to the ray for P-waves and perpendicular for S-waves. If the media contain interfaces, then the above formulation must satisfy the continuity of stress and displacement across these. When these interfaces are not smooth or two or more interfaces intersect at a point, then discontinuities arise in the zero order solution. The surface defining the discontinuity in U_o is the shadow boundary, and this divides the illuminated and shadow zones. ART is not applicable in the region surrounding the shadow boundary. Klem-Musatov (1984) and later Bakker (1990) have derived a formulation for diffracted waves valid in the vicinity of the shadow boundary, known as the shadow boundary layer. These diffracted waves smooth the discontinuities in zero order ART providing a valid twice differentiable solution throughout. The formula in the shadow boundary layer is

$$\mathbf{u} = U_o e^{i\omega\tau}\hat{\mathbf{e}} + W(w)\tilde{U}_o e^{i\omega\tau_d}\hat{\mathbf{e}} + O\left(1/\sqrt{\omega}\right), \qquad \text{(A-3)}$$

where τ_d is the diffracted wave eikonal, and

$$W(\omega) = \pm\frac{1}{2\sqrt{\pi}}\Gamma\left(\frac{1}{2}, -\frac{i\pi w^2}{2}\right)e^{-\frac{i\pi w^2}{2}},$$

where

$$w = \sqrt{\frac{2\omega(\tau_d - \tau)}{\pi}}. \qquad \text{(A-4)}$$

The incomplete gamma function is represented by $\Gamma(\frac{1}{2},z)$. The positive and negative signs are for the shadow and illuminated zones respectively. The variable w is a measure of distance from the shadow boundary (w = 0); since it is a function of the two eikonals, we must continue the geometrical wave eikonal τ by some method into the shadow zone, as it does not exist there according to the standard ray theory approach. It is worth remarking that the set of all points in space that satisfy $\tau = \tau_d$ defines the shadow boundary. The factor U_o does not exist in the shadow zone, being abruptly terminated at the shadow boundary, w = 0. $\tilde{U}_o$ represents the amplitude continued into the shadow zone, and is continuous across w = 0. Zero order ART has an accuracy of $O(1/\omega)$, however one can see from equation (A-3) that the error is of $O(1/\sqrt{\omega})$. We note in passing that this is the order of magnitude of the diffraction terms resulting from the geometrical theory of diffraction, which are not included in this equation. A graph of equation (A-3) is the solid curve in Figure 10, which shows the modulus of the amplitude of **u** using w as the

independent variable to get a frequency independent perspective. This can be contrasted with the dashed curve, which represents the amplitude of the geometrical wave, terminating at the shadow boundary. One can see that the diffracted wave contribution decays with distance from the shadow boundary, and is essentially negligible outside the boundary layer (shaded). The oscillations in the illuminated region are due to the interference between the geometrical and the diffracted waves.

Polarization

The direction of displacement (polarization) of the diffracted wave is parallel to that of the body wave it smooths. However, as Klem Mustatov (1994) notes, we can actually take the polarization parallel (or perpendicular, if we are dealing with S-waves) to the diffracted ray, as the difference is very small in the shadow boundary layer. We shall outline why this is true. Inside the boundary layer,

$$\tau \approx \tau_d + 1/2(m - m_d)p^2 \tag{A-5}$$

where p is the distance normal to the shadow boundary, m and m_d are the second partial derivatives in the direction normal to the shadow boundary, and $p = O(1/\sqrt{\omega})$ defines the boundary layer. We can write the gradient of τ and τ_d in ray coordinates, and from equation (A-5) we find that

$$|\nabla\tau - \nabla\tau_d| = O\left(1/\sqrt{\omega}\right) \tag{A-6}$$

and hence it follows that

$$|\mathbf{e} - \mathbf{e}_d| = O\left(1/\sqrt{\omega}\right). \tag{A-7}$$

This shows that the difference is negligible, since we have an error of $O(1/\sqrt{\omega})$ in the solution anyways. In our numerical example we take the polarization parallel and perpendicular to the diffracted rays for P-waves and S-waves, respectively.

Continuation of the Geometrical Eikonal

We noted before that τ doesn't exist in the shadow zone and must be continued there so we can make use of equation (A-3). One might at first be attracted by the simplicity of a plane wave continuation; however, this leads to significant errors. Technically this is incorrect since it is required that the solution be twice differentiable everywhere, and we can show that a plane continuation of the geometrical eikonal leads to a discontinuity in the first derivative at the shadow boundary. Specifically, for a proper solution we require

$$\left[\frac{\partial \mathbf{u}}{\partial p}\right] = 0 \tag{A-8}$$

where the large brackets denote the jump in the quantity across the shadow boundary, located at $p = 0$. After some expansion using equation (A-3), it becomes clear that this is equivalent to

$$\left[\frac{dW}{d\alpha}\frac{\partial\alpha}{\partial p}\right] = 0 \tag{A-9}$$

where $\alpha = i\pi w^2/2$. Using a plane wave continuation gives

$$\alpha = \begin{cases} 1/2i\omega p^2(m - m_d) \text{ in the illuminated zone,} \\ -1/2i\omega p^2 m_d \text{ in the shadow zone.} \end{cases} \tag{A-10}$$

Using equation (A-10) combined with the integral definition of the incomplete gamma function in equation (A-4), we quickly find that equation (A-9) is not satisfied for the plane continuation of the geometrical eikonal into the shadow zone. Although the solution itself is still continuous at the shadow boundary and the jump in the derivative may be quite small, the consequence of using a plane continuation of the eikonal turns out to be numerically significant. One can calculate the wave amplitude and compare it to the solution using a properly continued eikonal. The mismatch increases with distance from the shadow boundary, and exceeds 100% within the shadow boundary layer. Therefore the plane continuation of the eikonal is not suitable.

The simplest way to continue the eikonal is using equation (A-5); the wavefront curvature needs to be calculated at each point for the geometrical spreading, so this poses no additional burden. This was the method used in the Numerical Example section.

Continuation of the Geometrical Amplitude

Unlike the geometrical eikonal, a plane wave continuation of this parameter is valid. This is due to the fact that changes in U_o within the shadow boundary layer are of $O(1/\sqrt{\omega})$. Bakker (1990) derived equation (A-3) using the paraxial approximation, where U_o is the amplitude along the central ray, equivalent to a plane continuation of U_o in the shadow boundary layer. What is worth noting is that U_o contains a plane wave reflection/transmission coefficient for waves having encountered an interface during the course of their propagation. This then means that within the boundary layer differences in geometrical amplitude perpendicular to the shadow boundary are of $O(1/\sqrt{\omega})$, providing the reflection/transmission coefficient is not too rapidly varying (that is, we're not near critical or grazing angles). It can be shown that equation (A-3) satisfies the boundary conditions at a smooth interface to $O(1/\sqrt{\omega})$, when a plane wave continuation of the amplitude is used. If the interface is not smooth, then the edge wave formulation given in equation (A-3) is no longer valid for all the diffracted waves leaving the interface. A particular case of this was shown in the Numerical Example section.